Electronic Supplementary Material (ESI) for Journal of Materials Chemistry A.

Nanosized SnSb Alloy Confined in N-Doped 3D Porous Carbon Coupling with Ether-based Electrolytes toward High-Performance Potassium-ion Batteries

Zhiyuan Wang,*[a,b,c] Kangze Dong, [a] Dan Wang, [a,b,c] Shaohua Luo,*[a,b,c] Yanguo Liu, [a,b,c], Qing Wang, [a,b,c] Yahui Zhang, [a,b,c] Aimin Hao, [a,b,c] Chunsheng Shi, [d] Naiqin Zhao, [d]

[a] *School of Materials Science and Engineering, Northeastern University, Shenyang 110819, P.R. China;*

[b] *School of Resources and Materials, Northeastern University at Qinhuangdao, Qinhuangdao 066004, China;*

[c] *Key Laboratory of Dielectric and Electrolyte Functional Material Hebei Province, Qinhuangdao, China;*

[d] *School of Materials Science and Engineering, Tianjin University, Tianjin 300072,P. R. China*

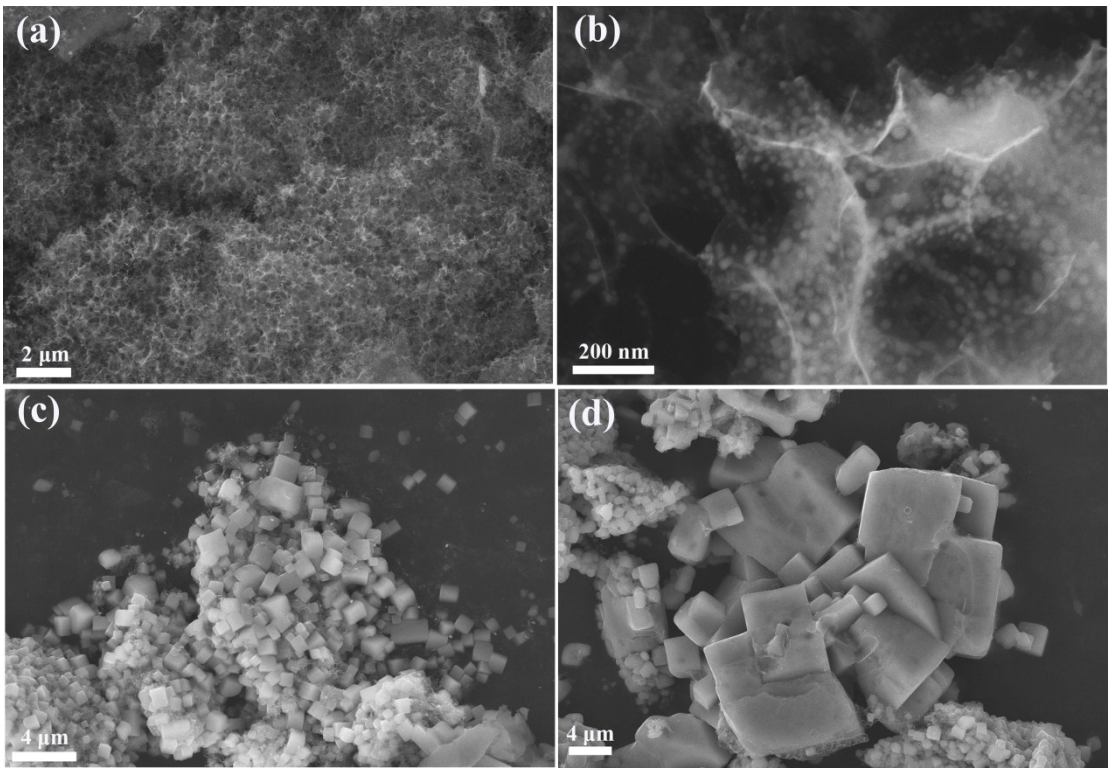

Fig. S1 (a, b) SEM images of 3D SnSb@NC alloy. (c, d) the 3D SnSb@NC alloy precursor.

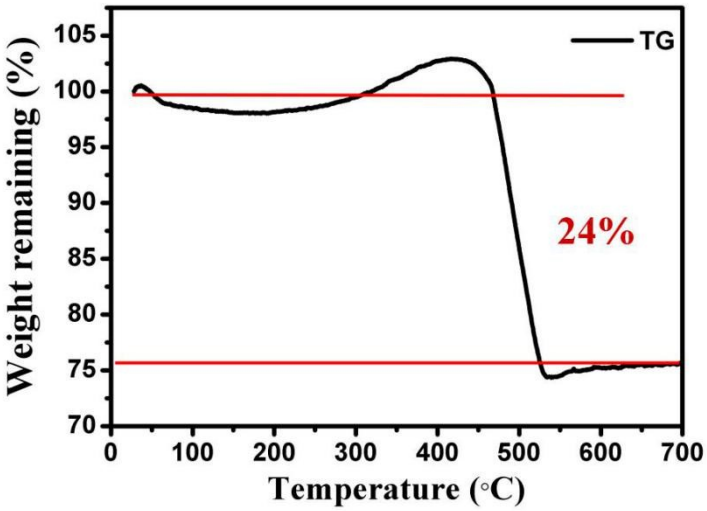

Fig. S2 TGA curves of 3D SnSb@NC alloy in air.

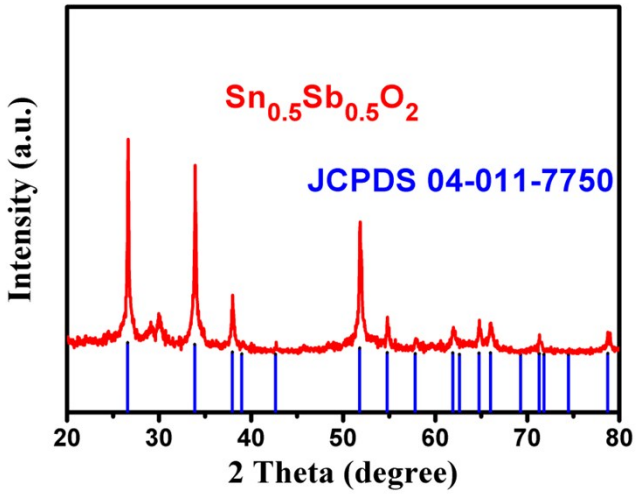

Fig. S3 XRD pattern of the 3D SnSB@NC alloy after TGA.

As seen from TGA curves (Fig. S1), the weight variation of 3D SnSb@NC alloy can be mainly attributed to the oxidation of SnSb alloy and 3D porous carbon during tests. The oxidation of SnSb alloy leads to a weight increase, while the remove of carbon leads to a weight decrease of the composites. As evidence by XRD after The TGA test (Fig. S2). The observed residual product can be index to tetragonal $Sn_{0.5}Sb_{0.5}O_2$ (JCPDS no. 04-011-7750). Based on the following equation, the mass fraction of 3D porous carbon in the composite is determined to be 40.03% :

$$SnSb + O_2 \xrightarrow{Air} Sn_{0.5}Sb_{0.5}O_2 \tag{1}$$

$$C + O_2 \xrightarrow{Air} CO_2 \uparrow \tag{2}$$

$$Carbon\ (wt\%) = \frac{initial\ weight\ of\ 3D\ SnSb@NC\ composite - M_{SnSb} \times \frac{final\ weight\ of\ product\ (SnSbO_4)}{M_{SnSbO_4}}}{initial\ weight\ of\ 3D\ SnSb@NC\ composite} \tag{3}$$

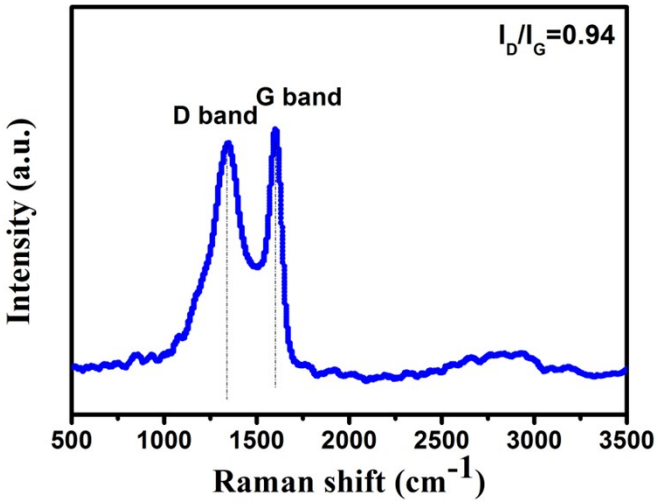

Fig. S4 The Raman spectra of 3D SnSb@NC.

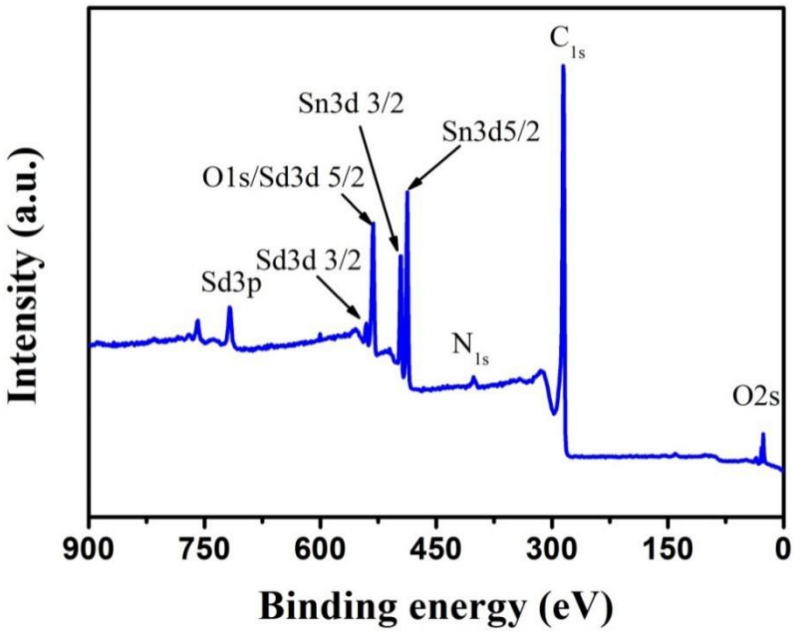

Fig. S5 The XPS full survey spectra of 3D SnSb@NC

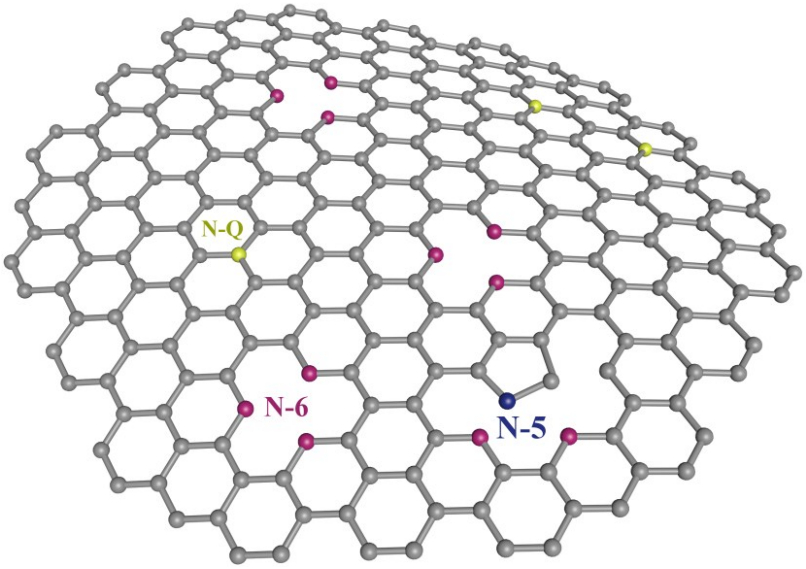

Fig. S6 Schematic illustration of three types of nitrogen defects in 3D SnSb@NC alloy: pyridinic N (N-6), pyrrolic N (N-5) and graphitic N (N-Q)

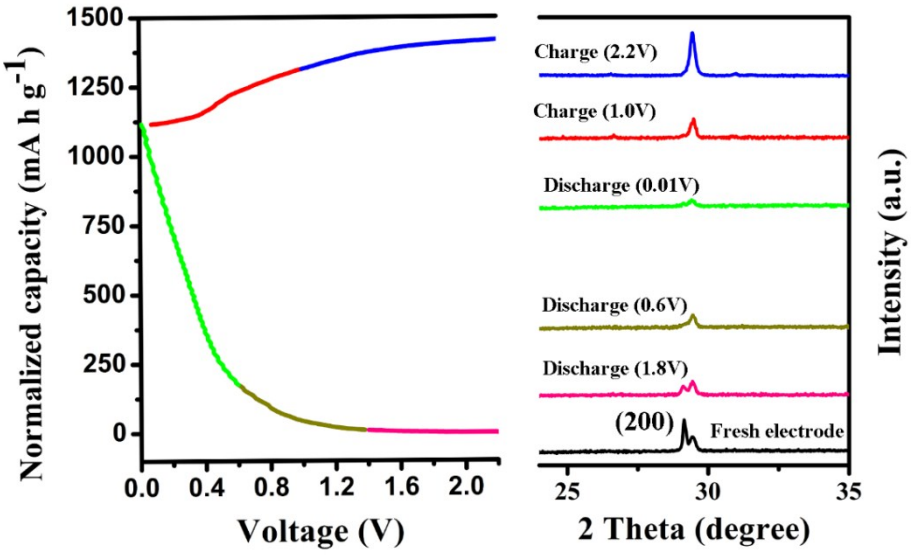

Fig.S7 Galvanostatic discharge-charge curves of 3D SnSb@NC electrode and its corresponding ex situ XRD images within a selected 2 range.

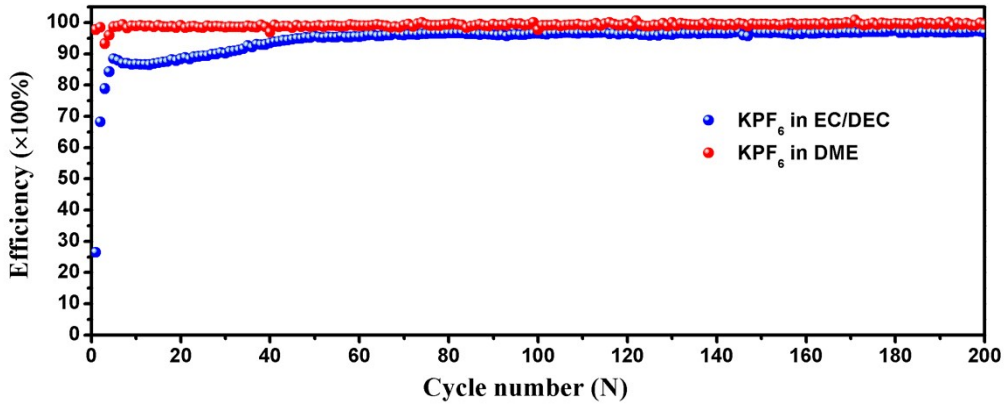

Fig. S8 Coulomb efficiency of long-term cycling of the cells with different electrolyte at 500 mA g^{-1}.

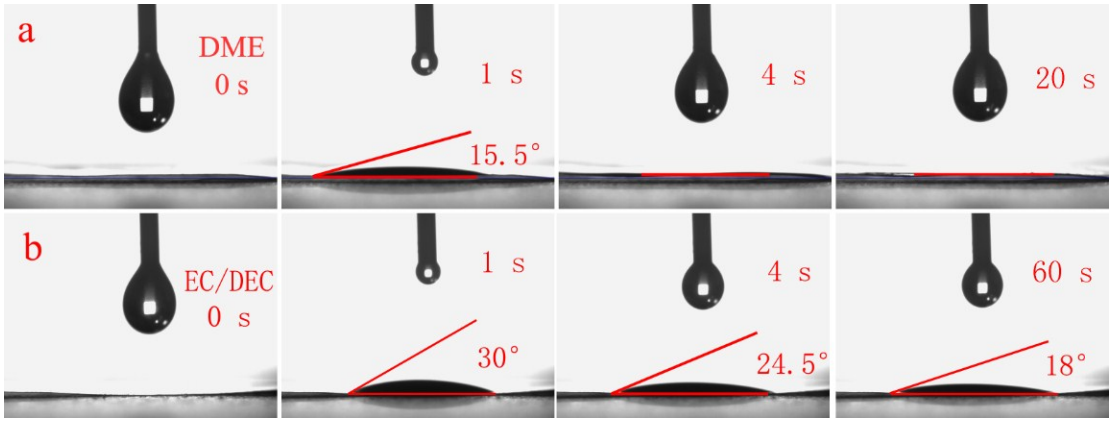

Fig. S9 Wettability of different electrolyte solvent on the 3D SnSn@NC electrode. (a) DME, (b) EC/DEC.

The electrochemical performance and specific capacity contribution rate of pure 3D carbon was also evaluated in EC/DEC and DME electrolyte, as shown in Figure S10. Specifically, as shown in Figure S10(a, b), the porous carbon electrode delivers reversible capacities of 132.9, 114.7, 99.9, 88.8 and 79.4 mAh g^{-1} at the current density of 0.1, 0.2, 0.5, 1 and 2 A g^{-1}, respectively. In comparison, a better rate performance was achieved in DME electrolyte (111.5, 106.3, 100.5, 98.3 and 97.7 mAh g^{-1} at the current density of 0.1, 0.2, 0.5, 1 and 2 A g^{-1}, respectively). Since the carbon content in 3D SnSb@NC composite material is about 40.03 wt.%, so the capacity contribution of 3D carbon is calculated as below in the overall capacity of the composite anode (Table.S1 and Table.S2).

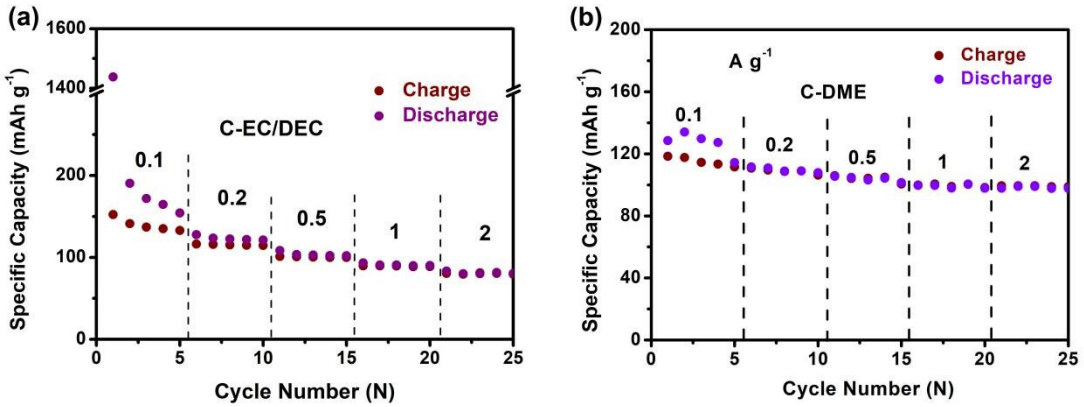

Figure S10.The electrochemical performance of porous carbon in (a) EC/DEC and (b) DME electrolyte.

Table S1. The value of the contribution of 3D carbon and SnSb in the overall capacity of 3D SnSb@NC anode in EC/DEC electrolyte.

Contribution percentage (%)	0.1 A g^{-1}	0.2 A g^{-1}	0.5 A g^{-1}	1 A g^{-1}	2 A g^{-1}
3D carbon	23.9%	23.2%	25.3%	26.2%	29.9%
SnSb	76.1%	76.8%	74.7%	73.8%	70.1%

Table S2. The value of the contribution of 3D carbon and SnSb in the overall capacity of

3D SnSb@NC anode in DME electrolyte.

Contribution percentage (%)	0.1 A g^{-1}	0.2 A g^{-1}	0.5 A g^{-1}	1 A g^{-1}	2 A g^{-1}
3D carbon	15.7%	15.5%	21.6%	25.4%	33.7%
SnSb	84.3%	84.5%	82.38%	74.6%	66.3%

Table S3 Electrochemical performance comparison of various K-ion alloy anodes

Anode materials	Current density (mA g^{-1})	Reversible capacity (mA h g^{-1})	cycles	Reference
Graphite	20	200	200	1
Co_3O_4-Fe_2O_3/C	50	203	50	2
Soft carbon	550	155	50	3
V_2O_3	50	210.7	500	4
SnS_2	25	250	30	5
Sn/C	25	110	30	6
Ti_3C_2 Mxene	200	50	900	7
MoS_2	20	65.4	200	8
Sn_4P_3/C	50	307.2	50	9
N-graphene	100	150	100	10
R-GO	100	170	100	11
TiS_2	24	151.1	120	12
3D SnSb@NC	**500**	**234.9** **185.8**	**100** **200**	**This work**

According to the literature[14], the micrometer-sized SnSb alloy particles was

prepared and investigated its structure, morphology, and electrochemical performance, as shown in the following (Fig.11). Pure-SnSb alloy electrode delivers an initial discharge/charge capacity of 433.2 and 286.6 mAh g^{-1} at 0.1 A g^{-1} in EC/DEC, respectively, with an initial coulombic efficiency (ICE) of 66.15%. After 20 cycles, the specific capacity rapidly decays to 25.7 mAh g^{-1}, which is due to the large volume change of SnSb during the potassiation/depotassiation, resulting in electrode pulverization. In comparison, pure-SnSb alloy delivers an initial discharge/charge capacity of 199.5 and 268.2 mAh g^{-1} at 0.1 A g^{-1} in DME with a higher ICE of 74.39%. In addition, a better capacity retention rate is achieved (212.3 mAh g^{-1} after 15 cycles) in DME.

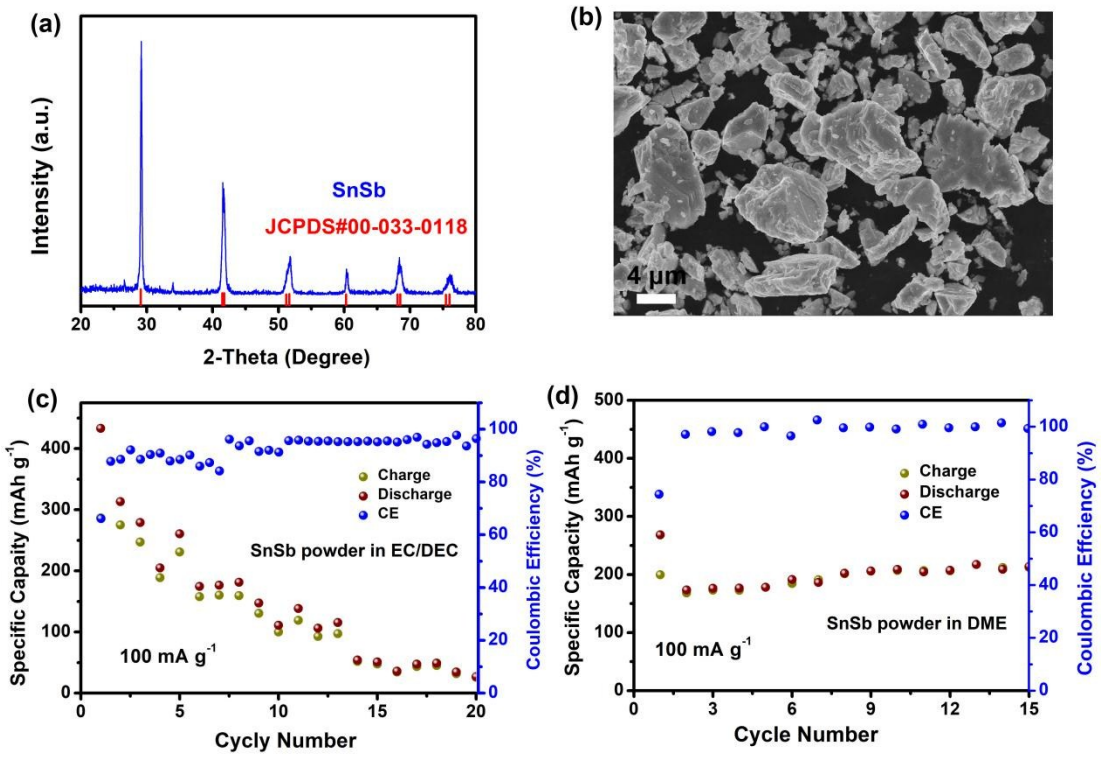

Figure S11. Pure-SnSb (a) XRD, (b) SEM, Cycle performance in (c) EC/DEC and (d) DME electrolyte.

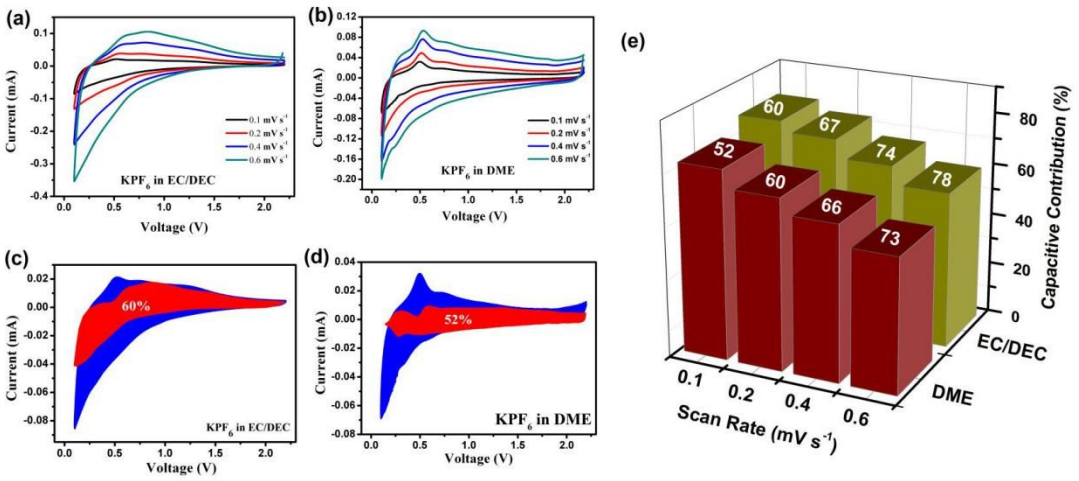

Fig. S12 (a, b) CV curves at different sweep rates and (c, d) capacitive (red) and diffusion-controlled (blue) contribution to charge storage at 0.1 mV s^{-1}, (e) the percentage histogram of diffusion contribution.

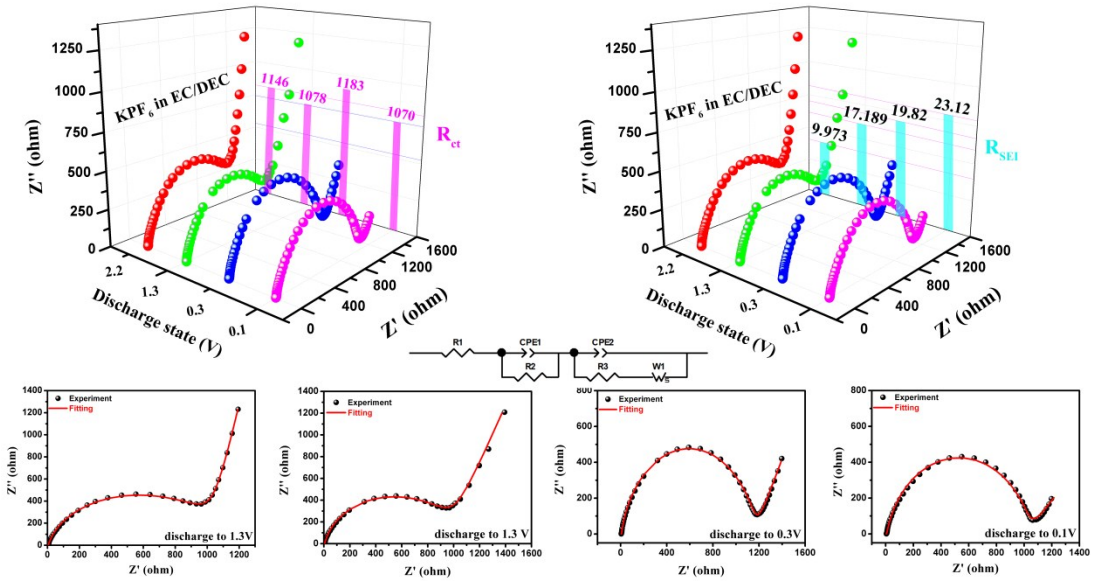

Fig. S13 The EIS analysis of 3D SnSb@NC at different discharge voltage in EC/DEC electrode and the corresponding equivalent circuit.

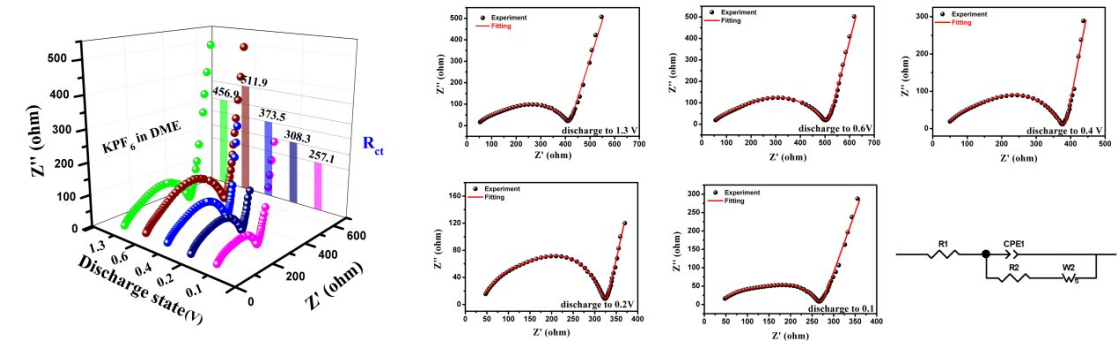

Fig. S14 The EIS analysis of 3D SnSb@NC at different discharge voltage in DME electrode and the corresponding equivalent circuit.

Fig. S13 and Fig. S14 compare the EIS spectra result for the 3D SnSb@NC electrode in various electrolyte solvent during the discharge process. The ex-situ EIS spectra and the corresponding equivalent circuit was obtain form a series of voltage points. The R_{ct} represent the charge transfer process. It is obviously that the values of R_{ct} of the 3D SnSb@NC electrode in DME solvent are smaller compared to electrodes in EC/DEC solvent, indicating that the electrode own relatively low resistance from charge transfer in DME solvents. In addition, the significant SEI films formation in EC/DEC solvents during discharge process. Notable, the R_{ct} values shows a trend of increasing first

and then decreasing during the ex-situ test. This may be due to the increased volume caused by alloying and the new substances produced that would extend the length of ions transfer pathway, thereby increasing the transfer resistance value[13]. However, with the gradual activation of the electrode, the resistance value in turn show a decreasing trend.

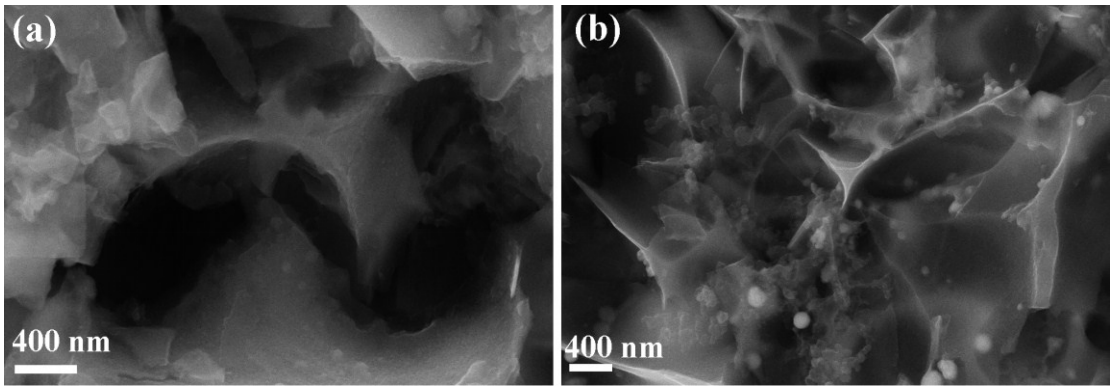

Fig. S15 SEM images of 3D SnSb@NC electrode after 30 cycles at 100 mA g^{-1} in different electrolytes: in (a) EC/DEC and (b) DME.

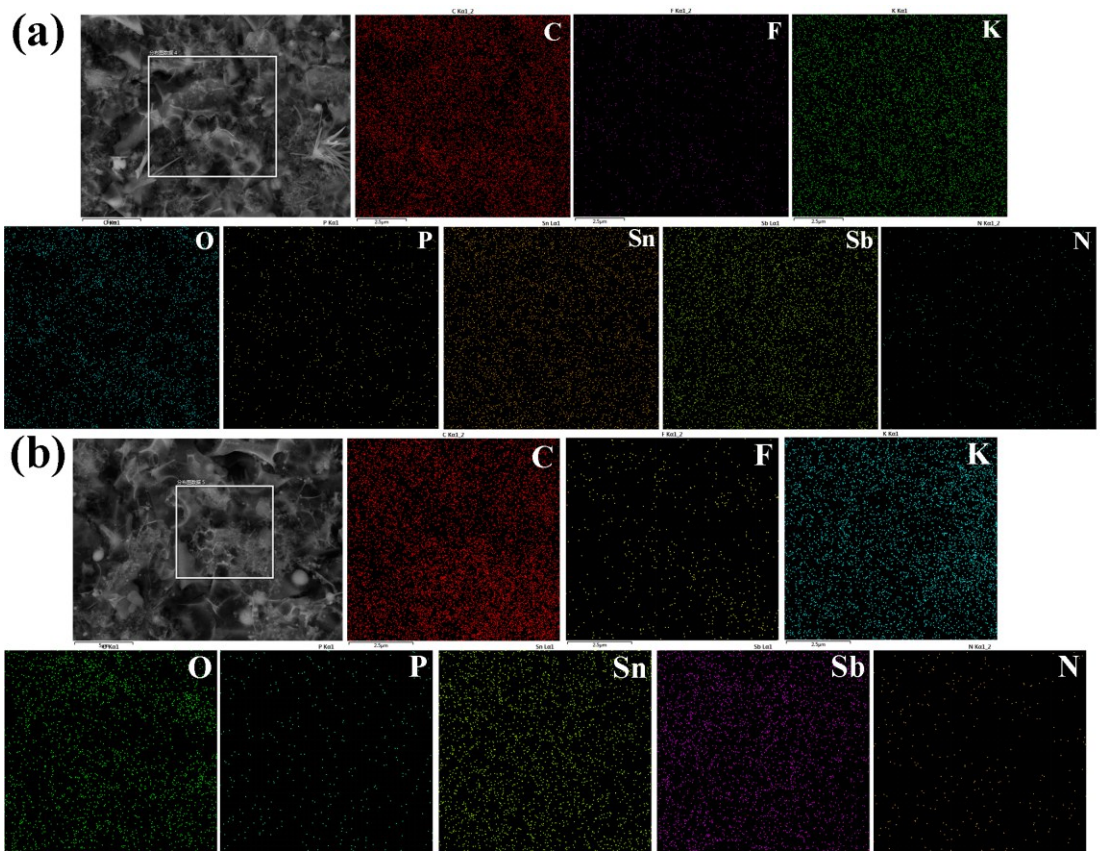

Fig. S16 The SEM image and EDS mapping of 3D SnSb@NC electrode after 30 cycles in different electrolytes: (a) EC/DEC and (b) DME.

Reference

[1] J. Zhao, X. Zou, Y. Zhu, Y. Xu and C. Wang, Advanced Functional Materials, 2016, 26, 8103-8110.

[2] Z. Jian, W. Luo and X. Ji, Journal of the American Chemical Society, 2015, 137, 11566-11569.

[3] I. Sultana, M. M. Rahman, S. Mateti, V. G. Ahmadabadi, A. M. Glushenkov and Y. Chen, Nanoscale, 2017, 9, 3646-3654.

[4] T. Jin, H. Li, Y. Li, L. Jiao and J. Chen, Nano Energy, 2018, 50, 462-467.

[5] V. Lakshmi, Y. Chen, A. A. Mikhaylov, A. G. Medvedev, I. Sultana, M. M. Rahman, O. Lev, P. V. Prikhodchenko and A. M. Glushenkov, Chemical Communications, 2017, 53, 8272-8275.

[6] I. Sultana, T. Ramireddy, M. M. Rahman, Y. Chen and A. M. Glushenkov, Chemical Communications, 2016, 52, 9279-9282.

[7] P. Lian, Y. Dong, Z.-S. Wu, S. Zheng, X. Wang, W. Sen, C. Sun, J. Qin, X. Shi and X. Bao, Nano Energy, 2017, 40, 1-8.

[8] X. Ren, Q. Zhao, W. D. McCulloch and Y. Wu, Nano Research, 2017, 10, 1313-1321.

[9] W. Zhang, J. Mao, S. Li, Z. Chen and Z. Guo, Journal of the American Chemical Society, 2017, 139, 3316-3319.

[10] K. Share, A. P. Cohn, R. Carter, B. Rogers and C. L. Pint, ACS Nano, 2016, 10, 9738-9744.

[11] W. Luo, J. Wan, B. Ozdemir, W. Bao, Y. Chen, J. Dai, H. Lin, Y. Xu, F. Gu, V. Barone and L. Hu, Nano Letters, 2015, 15, 7671-7677.

[12] L. Wang, J. Zou, S. Chen, G. Zhou, J. Bai, P. Gao, Y. Wang, X. Yu, J. Li, Y.-S. Hu and H. Li, Energy Storage Materials, 2018, 12, 216-222.

[13] S. Li, P. Ge, F. Jiang, H. Shuai, W. Xu, Y. Jiang, Y. Zhang, J. Hu, H. Hou and X. Ji, Energy Storage Materials, 2019, 16, 267-280.

[14] M. Walter, S. Doswald and M. V. Kovalenko, Journal of Materials Chemistry A, 2016, 4, 7053-7059.